Geophysical Prospecting, 1998, 46, 29-50

Estimation of reservoir fracturing from marine VSP using local shear-wave conversion[1]

Colin MacBeth,[2] Mark Boyd,[3] William Rizer[4] and John Queen[4]

Abstract

A marine VSP is designed to estimate the orientation and density of fracturing within a gas-producing dolomite layer in the southern North Sea. The overburden anisotropy is firstly estimated by analysing shear waves converted at or just below the sea-bed, from air-gun sources at four fixed offset azimuths. Full-wave modelling helps confirm that the background has no more than 3% vertical birefringence, originating from TIH anisotropy with a symmetry axis orientated perpendicular to the maximum horizontal compressive stress of NW-SE. This finding concurs with current hypotheses regarding the background rock matrix in the upper crust. More detailed anisotropy estimates reveal two thin zones with possible polarization reversals and a stronger anisotropy. The seismic anisotropy of the dolomite is then determined from the behaviour of locally converted shear waves, providing a direct link with the physical properties of its fractures. It is possible to utilize this phenomenon due to the large seismic velocity contrast between the dolomite and the surrounding evaporites. Two walkaway VSPs at different azimuths, recorded on three-component receivers placed inside the target zone, provide the appropriate acquisition design to monitor this behaviour. Anisotropy in the dolomite generates a transverse component energy which scales in proportion to the degree of anisotropy. The relative amplitudes, for this component, between the different walkaway azimuths relate principally to the orientation of the anisotropy. Full-wave modelling confirms that a 50% vertical birefringence from TIH anisotropy with a similar orientation to the overburden is required to simulate the field observations. This amount of anisotropy is not entirely unexpected for a fine-grained brittle dolomite with a potentially high fracture intensity, particularly if the fractures contain fluid which renders them compliant to the shear-wave motion.

[1] Paper presented at the 57th EAGE Conference – Geophysical Division, Glasgow, UK, May-June 1995. Received May 1996, accepted May 1997.

[2] Edinburgh Anisotropy Project, British Geological Survey, Murchison House, West Mains Road, Edinburgh EH9 3LA, Scotland, UK.

[3] Conoco UK, Aberdeen, Scotland, UK.

[4] Conoco Inc., Ponca City, Oklahoma, USA.

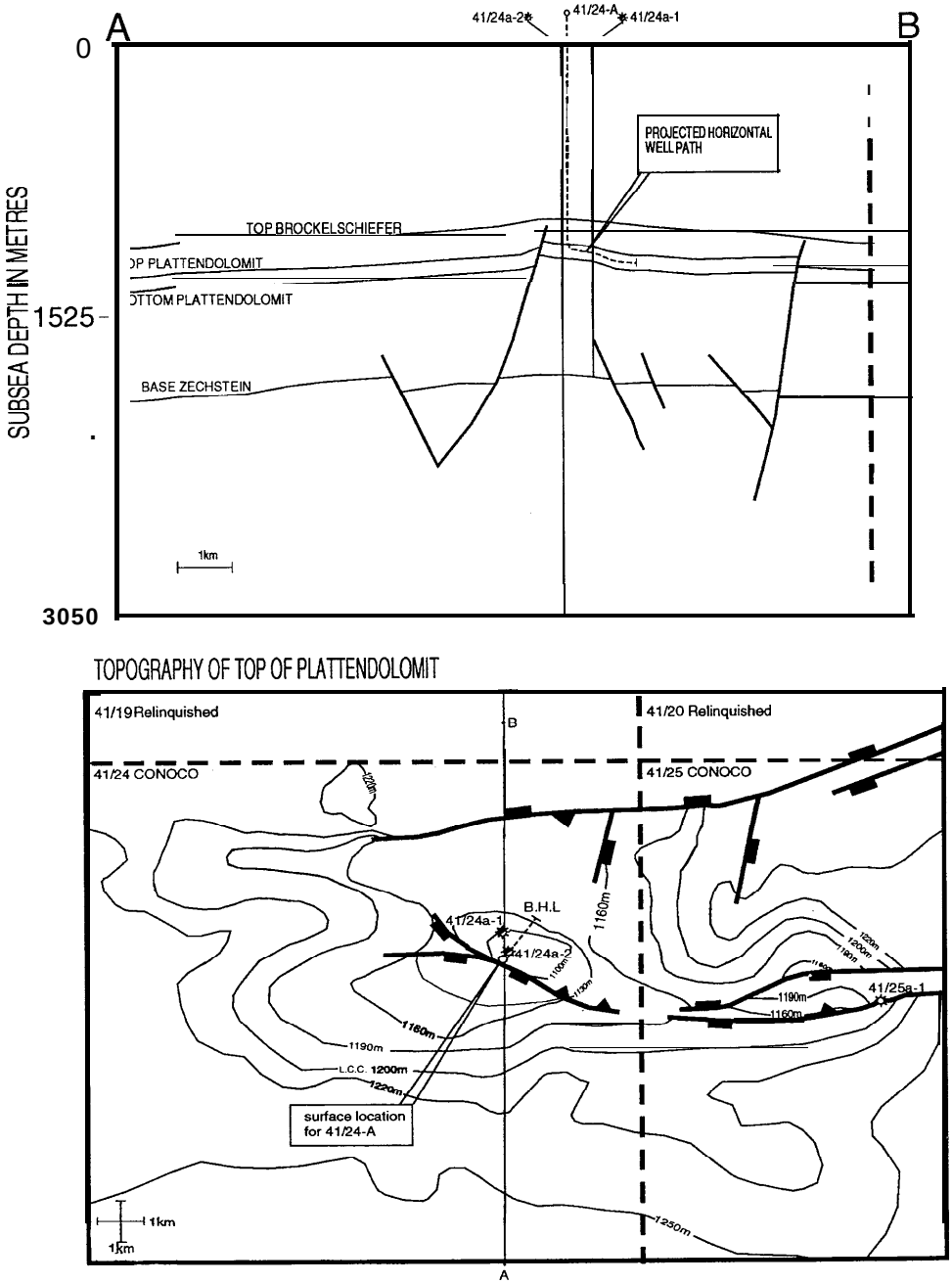

Figure 1. Vertical and plan views of the geological structure in the vicinity of the Plattendolomit target zone in the southern Gas Basin.

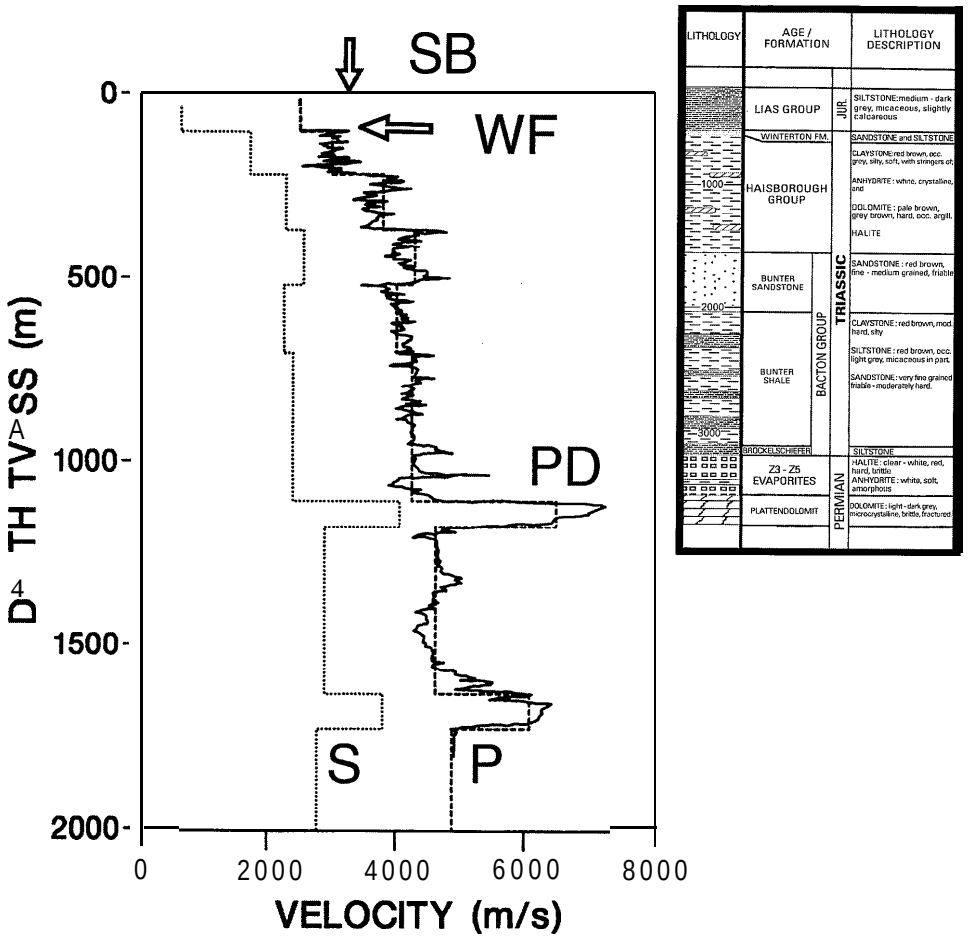

Figure 2. Velocity model used for full-wave modelling in this study superimposed upon the sonic log measurements and alongside the lithology taken from a neighbouring well. SB – sea-bottom; WF – Winterton formation; PD – Plattendolomit.

Introduction

At sea with seismic anisotropy

Over the past decade there has been a gradual increase in the resolution with which seismic anisotropy is measured. This has resulted from a combination of processing breakthroughs which focus on using the redundant information contained in multicomponent sources (Alford 1986), sampling at fine depth intervals (Lefeuvre *et al.* 1992), stripping the effects of overlying anisotropic layers (Winterstein and Meadows 199 1), or compensating for adverse effects associated with the near-surface and source imbalance (MacBeth *et al.* 1995). This combines with a growing awareness

that acquisition design is critical to a proper understanding of the anisotropy (MacBeth *et al.* 1993). Such advances have culminated in a number of higher resolution studies where shear-wave splitting can now be more directly interpreted as structure (Bruno and Winterstein 1994), or correlated with lithology and fluid flow (Horne and MacBeth 1995). Such detailed work usually uses multicomponent land sources.

Although multicomponent principles may, in theory, be transformed to the marine environment using a specialized acquisition geometry (MacBeth 1996), or the careful use of several select converted wave arrivals (Lefeuvre and Queen 1992), resolution is generally poor in comparison to land-based surveys. In general, the use of anisotropic techniques in offshore work still requires a fuller understanding of the variety of possible shear-wave conversions in the near- and subsurface (Ahmed 1990; Schruth, Bush and Digranes 1992). This current study addresses this requirement by presenting a technique which gives a local measure of the reservoir's shear-wave anisotropy using walkaway boat sources recorded on three-component receivers positioned inside the target layer itself. It relies upon a known local shear-wave conversion at the top of the reservoir formation, which gives rise to a measurable transverse component associated with the reservoir anisotropy. A similar phenomenon has been studied for the case of a reflection at an isotropic-anisotropic interface by Guest and Thomson (1992), and subsequently applied to upper mantle anisotropy.

0 bjec tive

The subject of the survey is a fractured carbonate reservoir, within the Upper Permian in the north-western part of the southern Gas Basin. The specific objective is to determine details of likely fracturing within a 76 m thick target layer at a subsea depth of 1106 m (Fig. 1). This layer is characterized by high seismic velocities, being encased in thick Zechstein evaporite sections with lower seismic velocities (Fig. 2), and is observed on surface seismics as a strong double event. A marine vertical seismic profile (VSP), designed specifically to utilize multicomponent seismic technology, was shot in January 1993 in a newly drilled well, with the planning for the experiment being carried out before the well was drilled. The design was based upon the proposed drilling track, which consisted of a vertical section with deviation into a short (500 m) N35°E horizontal section within the reservoir zone. Gas flow rates depend upon the ability to intersect large open fractures with the well-bore. Consequently, a horizontal well, designed to drill perpendicular to the expected orientation of the reservoir fractures, is anticipated to enhance productivity by encountering a number of large open fracture sets. With no direct evidence, fractures are expected to lie NW-SE, parallel to what is believed to be the present day regional maximum horizontal compressive stress (S_{Hmax}). This is also the orientation of the single fault observed in the seismic data. Conventional VSP will locate the Plattendolomit, but will give little information about the internal composition. The effects of shear-wave anisotropy measured from the multicomponent VSP can be used to infer the fracture direction and density. This is achieved by relating the shear-wave behaviour to the fractures by

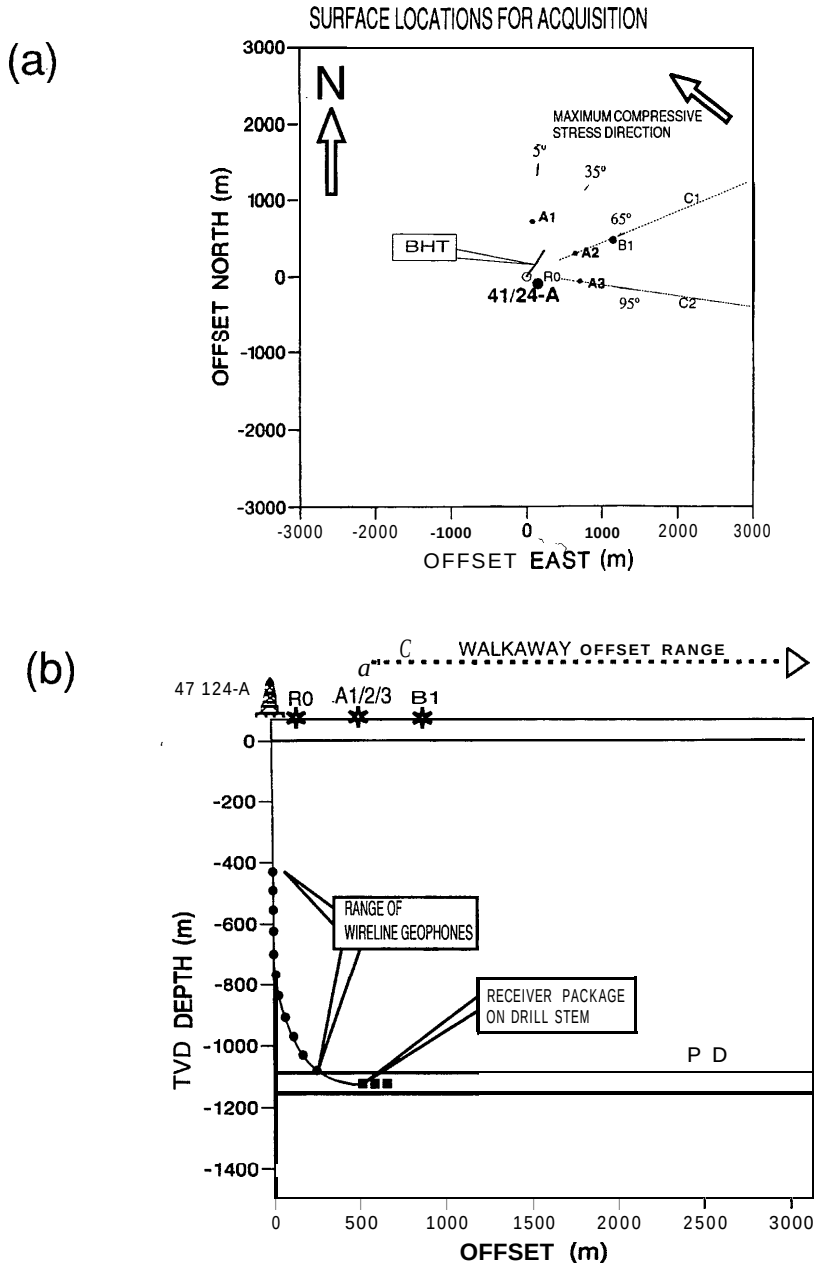

Figure 3. (a) Plan view of source lines for walkaway VSPs, horizontal projection of the wellhead and receiver position within the dolomite layer. (b) Vertical section showing all receiver tool positions for marine experiment, together with rig and boat offsets.

Table 1. Data acquisition parameters.

	Rig sources	Offset sources	Walkaway sources
Number of guns	$3\times100\,cm^3$	$2\times100\,cm^3$ $+2\times150\,cm^3$	$1\times300\,cm^3$
Arrangement of guns	cluster	cluster	cluster
Source depth	3 m	3 m	3 m
Azimuth	279" (near)	– 30°, + 30°, + 60" from BHT	+ 30°, + 60" from BHT
Offset relative to wellhead	56 m	700m Cl, C2, C3 1500m Bl	500 m-3200 m
Effective maximum frequency	200 Hz	200 Hz	200 Hz
Number of activations per receiver position	1		1
Downhole Sonde type		DESCO 3C receiver	
Depth locations	50 levels	50 levels	3 positions
Depth intervals		C1: 549 m–1116 m C2: 420 m–1116 m C3: 549 m–1116 m B1: 549 m–1116 m	1123m
Offset locations		700 m	500 m-3200 m

assuming that aligned fractures give rise to an equivalent anisotropic medium. This leads to a prediction based on the polarizations and time delays between split shear waves propagating within the Plattendolomit.

VSP acquisition

The design geometry is chosen from previous experience of optimal anisotropic surveying with land-based VSP in the Caucasus, Russia (MacBeth *et al.* 1993), combined with isotropic and anisotropic full-wave modelling for the model in Fig. 2. The velocity model in this figure is obtained by blocking the well log data into a small number of layers, with the shear-wave velocities being obtained using V_P/V_S values known for the different lithology (Tatham and McCormack 199 1). No attempt is made to introduce a TIV component of anisotropy arising from the velocity fluctuations in this model; the reasons for this not being necessary will become clear in later sections of this paper. The final configuration of acquisition components shown in Fig. 3(a,b) consists of three main parts (more specific details of the acquisition parameters are to be found in Table 1).

1 Rig source VSP: wireline receivers in the vertical section of the hole between 420 m and 1100 m TVD, record a rig source RO at 56 m offset.

2 Four offset VSPs: wireline receivers in identical positions to (1) record four offset source positions Al, A2, A3 and B 1. The minimum receiver depth is 549 m for offsets

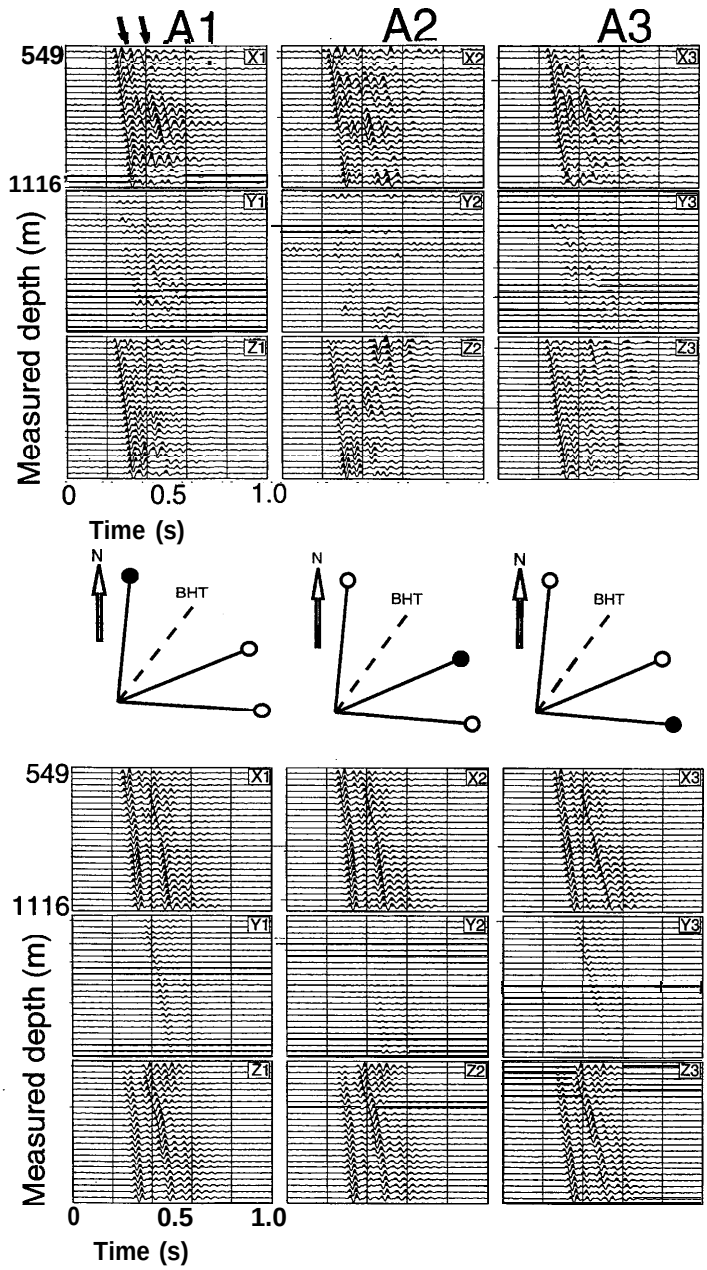

Figure 4. Observed three-component amplitudes for Al, A2 and A3 offset boat positions (top) together with full-wave synthetics (below). Observations and synthetics have been rotated into radial (X) and transverse (Y) directions. The traces are each scaled to the maximum vector norm for all levels. The recordings at receiver levels common to all three offsets, between depths of 549 m and 1116 m, are shown.

Al, A3 and B1, and 420 m for offset A2. The first three offsets are distributed at azimuths of N5°E, N65°E and N95°E on an arc of 700 m radius. B 1 is at a larger offset of 1500 m, with an azimuth of N65°E.

3 Two walkaway lines: a single three-component receiver package located inside the Plattendolomit, at 500 m, 530 m and 560 m offsets, along the horizontal section of the hole, records increasingly offset source positions which move, in turn, along two lines drawn radially outwards from the wellhead. The offsets vary between 500 m (near normal incidence) and 3200 m, and have azimuths of N65°E (Cl) and N95°E (C2). The receiver package is conveyed into the hole using the drill pipe.

The rig source VSP provides reference data for the velocity structure and tool coupling. The offset VSPs provide information about the anisotropic properties of the overburden from converted shear waves generated at the sea-bottom and near-surface interfaces. The walkaway VSPs are designed to record seismic wave energy affected by the high-velocity Plattendolomit layer, from which details of the fractures within this target zone may be inferred. A locally converted shear wave, which will carry information about the fracture-induced seismic anisotropy, is expected, due to the large seismic velocity contrast. Although both offset and walkaway information are necessary to build up a composite picture of the anisotropic structure for modelling, we shall see later that the fracture estimation does not rely upon the overburden properties, and these can be used in isolation from other measurements. The overburden anisotropy does, however, boost confidence in our final interpretation.

Estimation of overburden anisotropy using offset VSPs

Figure 4 shows a data matrix display of three-component recordings from the three separate groups of source activations at offsets Al, A2 and A3. Each has been corrected so that the motion is referred to a local set of receiver axes aligned along the in-line (radial (X), away from the wellhead) and cross-line (transverse (Y)) directions for each source-receiver line azimuth. This compensates for the inevitable twisting of the sonde in the borehole during acquisition. Fortunately, this operation need only be applied to a rotation about the vertical (Z) axis as the receiver package is gimballed so that one component is directed along the true vertical, even in the deviated portion of the well. This horizontal misorientation can be corrected by straightforward premultiplication of each amplitude vector by a rotation matrix, $\mathbf{R}_Z(\theta_i)$, implementing rotation about the Z-axis (see the Appendix for the definition of $\mathbf{R}_Z$). It is usual to estimate θ_i for each source-receiver line using the P-waves. Misorientations are estimated by windowing the initial, mostly linear, segment of the P-wave, then performing an eigenanalysis on the covariance matrix formed by the three-component motion. Assuming that this motion lies entirely within the sagittal plane, this automatically yields θ_i. We find that the θ_i estimates determined from the three separate sources, at each common receiver level, agree with each other to within a few degrees. This further suggests that the surveyed area may not possess any large

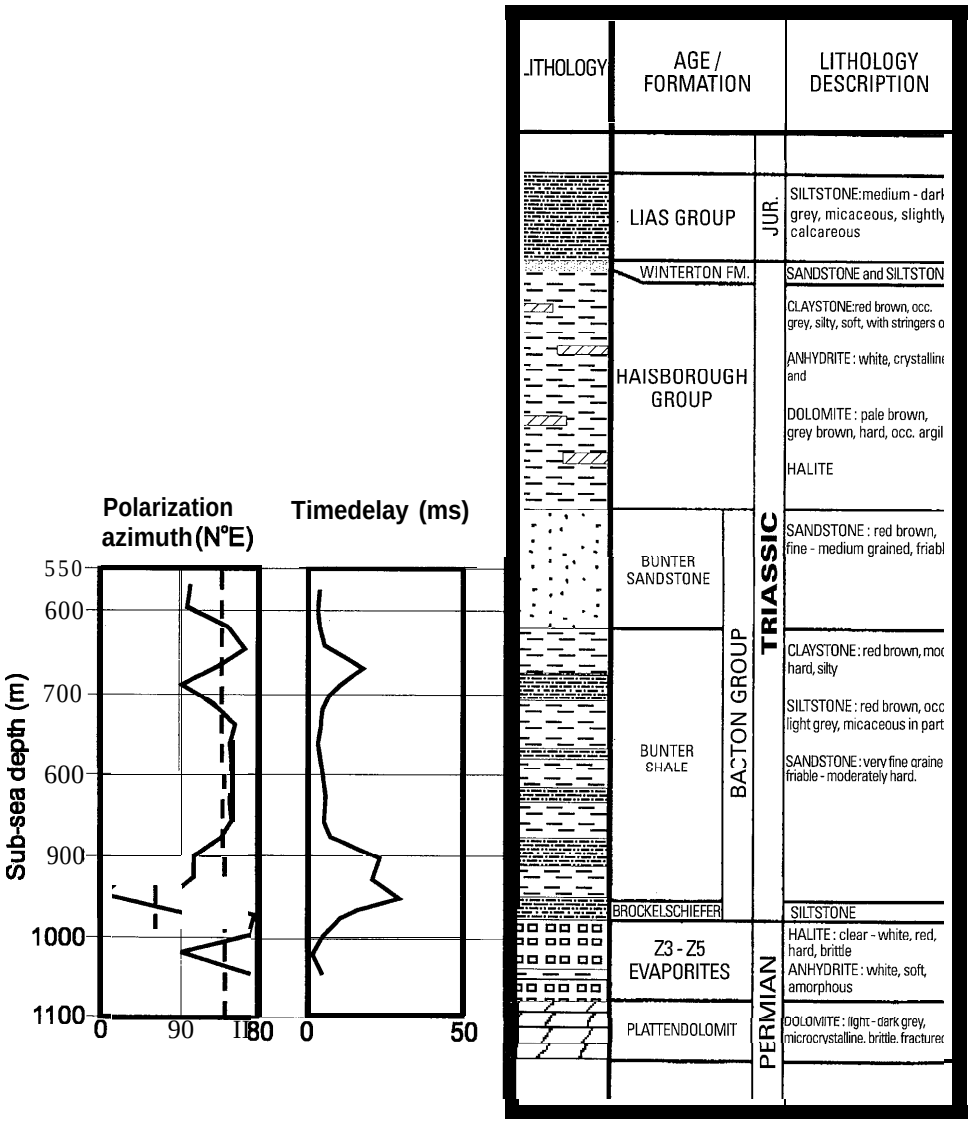

Figure 5. Average anisotropy estimates for the three offset data sets compared with the lithology. The dashed line on the polarization diagram is perpendicular to the maximum compressive stress, and is shown for reference. The polarization azimuth is for the qS1 wave.

structural dips. A further cross-check is possible using gyroscope orientation information recorded from an additional wireline run for the A2 boat position. These results confirmed an accuracy to within 5° using the P-waves for the reorientation.

The data from all three offset source locations display converted shear waves, marked by the arrows in Fig. 4. The converted shear waves originate from the bottom of the Winterton formation (WF), at the interface between siltstone and claystone (see Fig. 2), with slower arrivals originating from, or close to, the sea-bed. This interpretation, and the anisotropic behaviour, is confirmed by modelling with the anisotropic reflectivity method (Taylor 1987). The results of this full-wave modelling are shown in the lower picture of Fig. 4. The energy of the mode-converted shear waves places a tight constraint on the V_P/V_S of the siltstone (V_P/V_S = 2.2). The transverse component energy appears strongest for the Al offset followed by A3, but is weaker for A2. Although the modelling cannot determine accurate values, if this anisotropy were fracture induced, the fracture normals would lie 10" east of the borehole trajectory close to the source-receiver line for A2. This observation indicates that the A2 source does not excite the faster split shear wave (it has a cross-line polarization in this case), and that the offset azimuth lies close to the perpendicular to the expected NW-SE fracture direction. This particular interpretation is valid provided the raypath directions lie within the band of parallel horizontal polarizations defined by the line singularity (for a TIH medium) or point singularities (for an orthorhombic medium). The geometry of the acquisition indicates that this interpretation may be the case for the deeper levels, although modelling also demonstrates that this may be more widely applied. It is interesting to note that the observations from source B 1, offset 1500 m along the same line (not shown), appear to show a similar behaviour to the A2 offset.

Quantitative analyses of the shear waves are also possible by treating the three-component amplitude vector from each line azimuth either separately in a single-source method (Zeng and MacBeth 1993) or together (MacBeth 1996). Figure 5 shows the final averaged anisotropic measurements alongside the corresponding lithology. There appears to be a consistent polarization direction of N140°E for the faster split shear-wave polarization (solid line) for the middle section of the Bunter shale, lying close to the S_{Hmax} (dotted line), with fluctuations about this value at the top and bottom of the formation. The time-delay estimates show two zones of high time delay, the first building up to 15 ms (25% anisotropy) at the top of the Bunter shale. This occurs again with an increase to 25 ms (40% anisotropy) close to the bottom of the Bunter shale, before the transition into the Brockelschiefer and evaporites. Azimuthal isotropy (TIV anisotropy) in the shale layer cannot explain this variation as the raypaths are subvertical and the layer is subhorizontal. Numerical modelling reveals that differently polarized reflections from the dolomite layer are too weak to interfere with the shear-wave arrivals, and hence could not contribute to this time-delay peak. Large time delays indicate strong birefringence and may relate to lithological or fracture-dependent changes, or to intense fracturing (Horne and MacBeth 1995). It is possible that the deeper delays could be linked to the evaporites. As the seismic anisotropy can help identify pure salt (higher anisotropy) and recrystallized salt (lower anisotropy) in the anhydrite, it may provide indirect information about the evaporite sequence (Sun *et al.* 199 1). Unfortunately there were

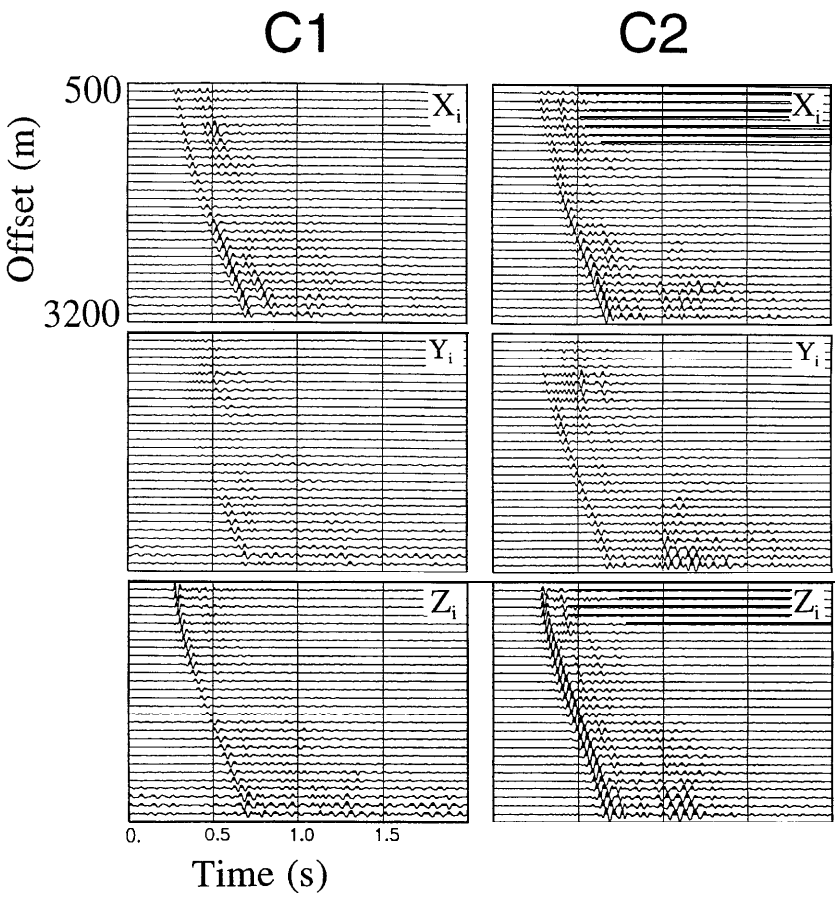

Figure 6. Observed walkaway data vectors for lines Cl and C2, with low-pass filter at 50 Hz applied (for modelling purposes), and normalization as in Fig. 4. Each three-component displacement vector has again been rotated so that the X-component is radial and the *Y*-component is transverse. This has been adjusted using the known acquisition geometry.

insufficient data points lying within the evaporites to deduce a satisfactory correlation, and a common origin for both features, associated with the shales, may be a more satisfactory conclusion. The time-delay peaks indicate a sharp change of polarization at the top and bottom of the Bunter shale, followed by an equally rapid reversal. The time delays throughout the remaining portion of the Bunter shale are small (2-5 ms) above the shallowest peak, being consistent with our expectations that the general rock matrix in the upper crust may be explained by a weak 1–3% anisotropy. These values are also consistent with that required for the full-wave modelling of the total wavefield. These values are small in comparison to path-averaged values of 10% to 15% for large discrete cluster sets in reservoir zones such as the Austin Chalk in Texas

(Mueller 1991), but quite typical for matrix values for most materials in the upper few kilometres of the crust.

Observation and analysis of locally converted shear waves in the walkaway data

Acquisition geometry and tool rotation

A single three-component receiver package is conveyed on the drill stem and positioned at three closely spaced (30 m apart) locations within the Plattendolomit (Fig. 3b). Six walkaway VSPs are then shot with offsets ranging between 500 m and 3200 m from the rig, with the boat source firing approximately every 25 m. This boat moves along the two different azimuthal lines C 1 and C2 at N65°E and N95°E, firing into each receiver position in turn. Due to the offset of the horizontal well, raypath and line azimuths deviate for the smaller source offsets, but begin to converge beyond 750 m, eventually becoming a few degrees apart. Tool rotation based upon the P-waves may be applied again to adjust the recorded vector amplitudes into local coordinate systems with in-line and cross-line directions corresponding to each source-receiver pair. However, as the walkaway is a common-receiver gather, these rotation angles can also be determined by the fixed acquisition geometry. We find agreement between these two procedures for small- to mid-offsets, confirming the quality of the incoming signals, but a divergence at the further offsets.

Locally converted shear-wave?

During the rotation procedure it is also observed that although the P-wave motion in the horizontal plane is initially linear and radial, it becomes increasingly elliptical and finally quite circular with increasing offset. The results of this behaviour can be clearly observed in Fig. 6, which shows the vector amplitudes for both lines which have been rotated using estimates from the acquisition geometry. Although several other wavetypes may be generated by the thin dolomite layer, it is most likely that the strong systematic increase in the transverse (Y) component of motion can be explained by the arrival of qS-waves converted locally from the top of the Plattendolomit, with polarizations controlled by the anisotropic properties of the Plattendolomit. This is an efficient conversion as V_S for the Plattendolomit matrix is quite close to V_P in the overburden because of the high seismic contrast.

Identification of the converted shear waves is based upon consideration of the various other possible wave types generated at the dolomite layer. Unlike low-velocity layers which trap a large proportion of energy as normal-mode dispersive channel waves, high-velocity layers cannot effectively establish channel waves due to leakage of energy into the surrounding rocks. The P-waves reach the receiver by refraction at small offsets (Fig. 7a), but at larger offsets beyond their critical incidence, the converted (refracted) shear wave is produced together with overcritically reflected P-waves and an inhomogeneous P-wave which tunnels into the thin layer. The P–qS

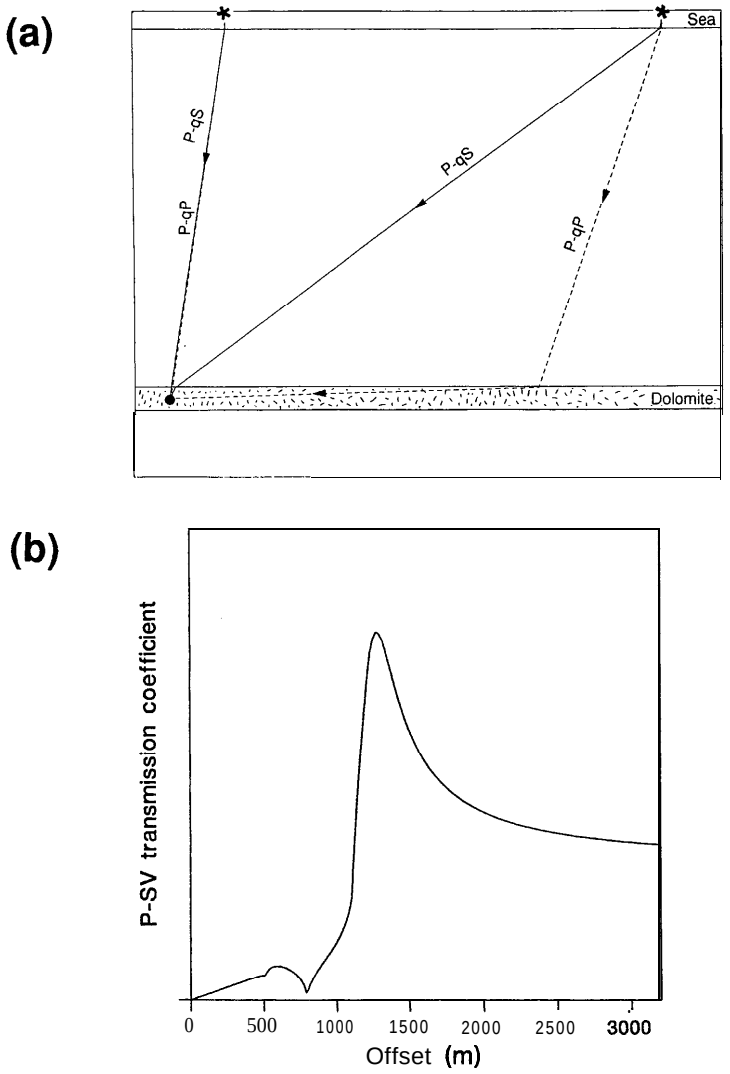

Figure 7. (a) Refracted raypaths relevant to the local conversion phenomenon at the anisotropic dolomite layer. P–qS is significant at large offsets. (b) Conversion coefficient between P- and SV-waves for an isotropic (evaporite)-isotropic (dolomite) interface with the current geometry determining the offset.

refraction point lies close to the receiver location and the critical angle cannot be exceeded at our experiment offsets. The conversion coefficient becomes prominent beyond the P-P critical angle, at an approximate offset of 1250 m (Fig. 7b). The amplitude of the tunnelling wave decreases with increasing frequency, angle of incidence, and vertical distance from the interface (Fuchs and Schultz 1976).

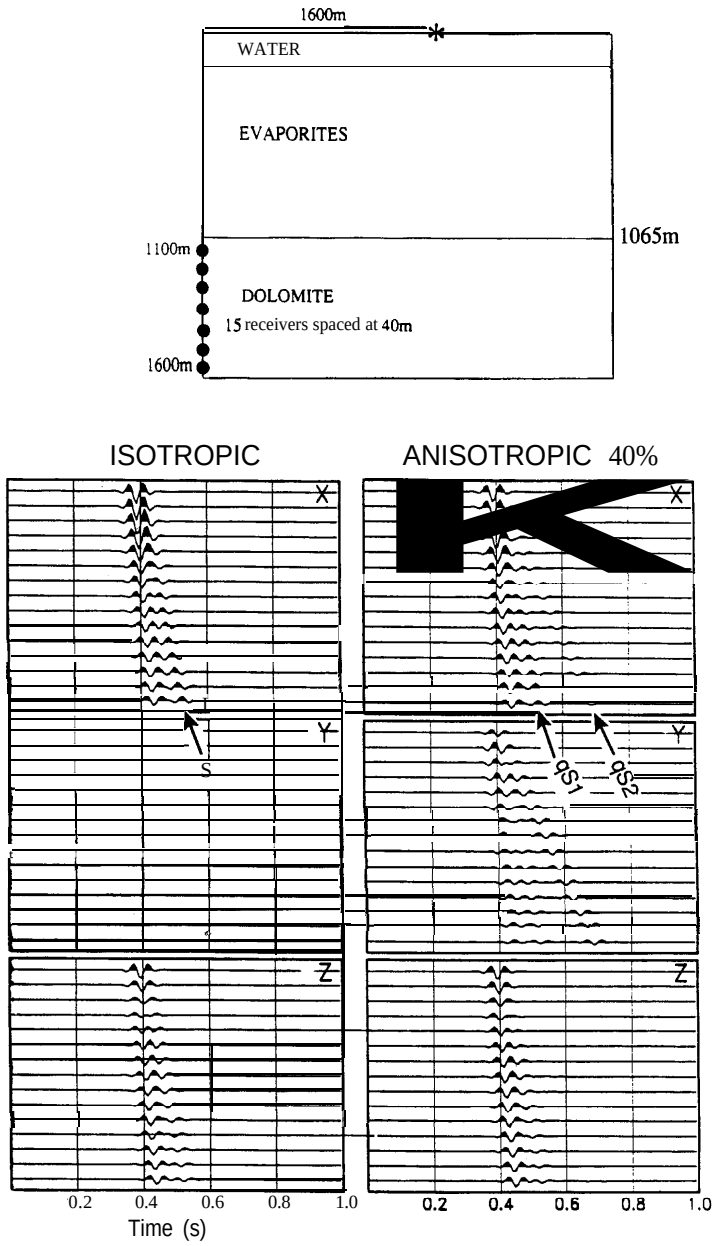

Figure 8. Full-wave synthetic seismograms for an isotropic and anisotropic dolomite half-space, highlighting the development of the local shear-wave conversion with penetration into the high-velocity layer. Note the large difference in qS1 and qS2 moveouts for the case with large anisotropy.

Fortunately, it maintains a similar horizontal polarization to the incident wave, and is thus unlikely to be confused with the shear wave. A P-head-wave is present only at high frequencies, as its wavelength must be several times smaller than the layer thickness.

A flat isotropic layer alone cannot explain the tranverse component as a converted SV-wave would possess a polarization confined to the sagittal plane. Another alternative cause is P-wave side-scattering by some lateral variation in velocity or structure. This is not considered, due to the regularity of our observation for all recordings along both lines, combined with the geological evidence suggesting horizontal layering in the vicinity of the surveys. Cross-coupling between receiver components could also be considered, although observations show that the elliptical motion does in fact consist of a distinct second arrival. To confirm further our interpretation of the local conversion and identify the converted shear waves, we apply full-wave modelling using the anisotropic reflectivity method. P-waves incident upon a half-space of dolomite from overlying water and sediment layers are considered. Receivers are distributed in a vertical array lying 35 m below the sediment-dolomite interface, each being separated by 40 m (Fig. 8). The dolomite is taken firstly as isotropic, and then 40% TIH anisotropic with a symmetry axis orientated at N45°E. Both sets of seismograms reveal clear converted waves arising from the P-wave, and highlight the small delays between the arrivals at the depth relevant to our present study.

Evaluation of fracture details

The transverse component amplitude u_Y is due to a mixture of converted qS1 and qS2 waves. It is formed by the sum of the projected motions, and is very sensitive to the Plattendolomit anisotropy, but is also dependent upon the direction of propagation. Applying (Al) to the conversion at the top of the Plattendolomit, u_Y can be written as a function of the source-receiver offset r,

$$u_y(r,t) = a_{\mathrm{p}}\, T_{\mathrm{P-SV}}(r)\sin\beta(r)\cos\beta(r)\,\{\, s_2(t) - s_1(t)\,\} \qquad (1)$$

where the polarization azimuth β of the qS2 wave in the plane normal to the raypath relates to its measured horizontal projection α_{H} and angle of incidence θ via the relation in the Appendix, and $s_1(t)$ and $s_2(t)$ are delayed wavelets corresponding to the two split shear waves, respectively. The term a_{P} represents the incident P-wave amplitude at the evaporites-dolomite interface, and contains the geometric spreading and transmission coefficients for the overburden. The dependence on the dolomite anisotropy is controlled by the last two factors in (1).

A practical measure of the magnitude of the transverse component may be taken by forming the quantity $v_Y = \langle u_Y(t)^2 \rangle^{1/2}$, where the angled brackets refer to an average over a time window including all the arrivals. Assuming a one-cycle sine wave for the source wavelet and rearranging the equation, we obtain

$$v_Y(r) = k(r)\, T_{\mathrm{P-SV}}(r)\delta t D \sin\alpha_{\mathrm{H}}(r)\cos\alpha_{\mathrm{H}}(r)/(\cos^2\theta\cos^2\alpha_{\mathrm{H}}(r) + \sin^2\alpha_{\mathrm{H}}(r)) \qquad (2)$$

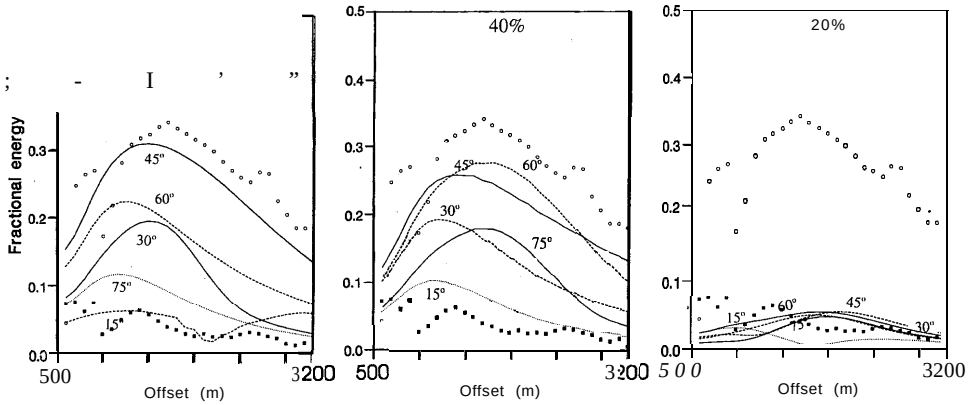

Figure 9. The fractional energy ν_Y on the transverse component of the walkaway VSPs normalized by the vector amplitude at the minimum offset. Lines are determined using full-wave modelling for different acquisition azimuth orientations ϕ relative to the fracture normal, and for 50%, 40% and 20% vertical birefringences. Topmost symbols correspond to walkaway C2, and the others to walkaway C 1, with these observations relating to Fig. 6.

where δt is the time delay per unit length, D is the depth of the receiver in the layer, θ is the propagation angle inside the layer (smaller than the angle of incidence due to refraction), and α_H is the horizontal polarization of the qS1 wave. This result also holds for other wavelets, but with differing constants of proportionality. From this equation we see that adequate shear-wave conversion is required before ν_Y becomes significant, although once established, the variation with offset and azimuth is essentially controlled by the anisotropy.

The overall magnitude of the time delays determines the general sensitivity to the anisotropy, and ν_Y displays a systematic variation with azimuth for most offsets. For offset lines parallel or perpendicular to the polarization directions, α_H = 0" or 90°, ν_Y is zero.

Figure 9 shows ν_Y predicted for 50%, 40% and 20% vertical shear-wave birefringence, and for offset azimuths of 75°, 60°, 45°, 30" and 15" relative to the symmetry axis of a TIH anisotropy. These curves are generated using full-wave synthetics owing to various ray-bending effects which influence the composite value. They are normalized by the value at the lowest offset (500 m). The elastic constants for such large anisotropies are simulated by an equivalent medium formed by alternating vertical plates of soft and hard material. The relative magnitudes of the elastic constants generated by this approach do differ from that obtained using fracture systems with more appropriate boundary conditions, and the method must be treated here as one way of obtaining a sufficiently high vertical birefrigence. As the offset geometry for the two lines Cl and C2 are directly comparable, $T_{P\text{-}SV}$ remains the same and the amplitude variations may be used to determine the anisotropy. Estimates for ν_Y obtained from the observations are also

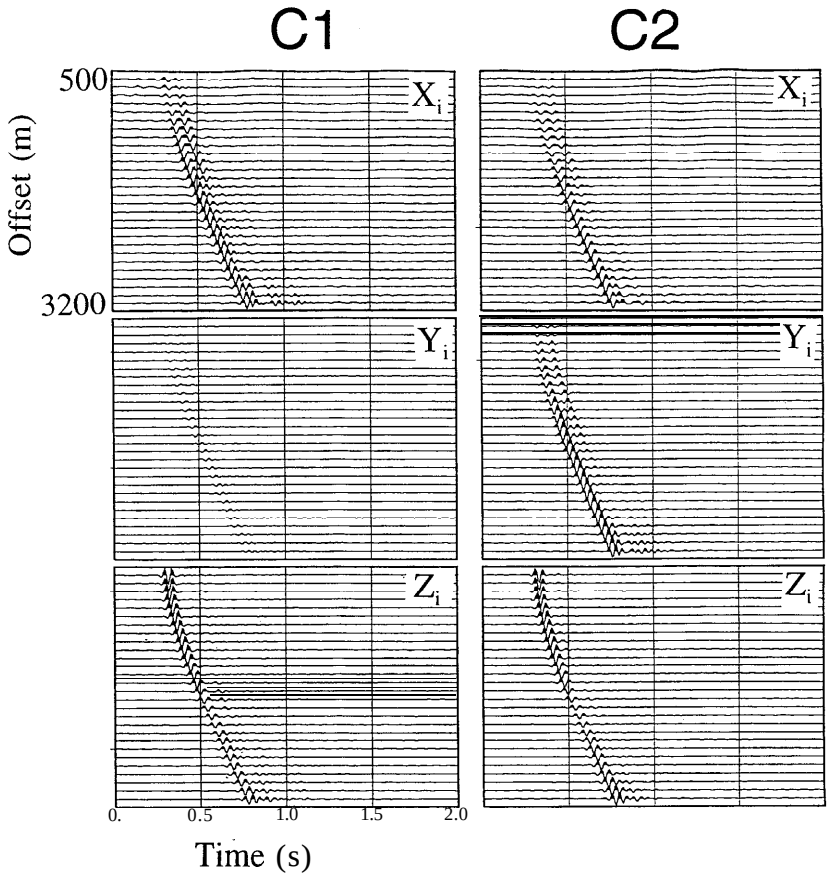

Figure 10. Final synthetic seismograms which should be compared with the observations in Fig. 6. Relative amplitudes are fixed by the 50% TIH anisotropy with a symmetry axis at N50°E. It is possible that the observations in Fig. 6 may indicate a change in orientation towards the east at larger offsets.

overlain on this plot. This clearly shows that the Cl amplitudes are much lower than those for C2, with the particular variation being closer to the predictions corresponding to the 15" and 45" curves for the 50% anisotropy. This also appears in agreement with the line azimuth difference of 30" in the acquisition. The result suggests that the azimuth of the symmetry axis (normal to the fracture strike) lies 15" west of the Cl line (i.e. N50°E). As a final check for these results, we construct the synthetic seismograms shown in Fig. 10, which should be compared with the observations in Fig. 6. From this comparison process, it appears that fracture normals lying 10" to 15" east of borehole trajectory fit the observations, corresponding to a fracture strike of between N135°E and N140°E. There are some indications of fluctuations around these results, with a small increase in the transverse component

energy on Cl at large offsets (Fig. 6) indicating the possibility of a change in orientation towards the east further from the borehole.

Discussion and conclusions

Results and interpretation

Fracturing in the Plattendolomit may be related to overpressure and uplift accompanying the Late Cretaceous/Early Tertiary inversion of the Cleveland Basin. It is likely that the thick salt sections above and below the Plattendolomit promoted the development of overpressure by sealing, in pressures upon uplift. The over-pressure in uplift may have caused regional fracturing as well as local fracture enhancement around reactivated fault zones. Reserve estimates assume that fractures are restricted to areas surrounding the fault zones, and two wells in the immediate vicinity of the survey site are marginally productive (Fig. 1). Our seismic anisotropy estimates can penetrate several hundred metres beyond the well, and appear to suggest mainly a uniform fracture spacing with a possible fluctuation towards the end of the C 1 line.

The results of the seismic anisotropy study indicate that the normal to the predominant Plattendolomit fracturing is directed along N50°E, with a corresponding fracture strike subparallel to the expected present day regional stress direction of NW-SE. This conforms with stress orientation determined for the Plattendolomit from analyses of FMS and caliper logs in nearby wells. There is a departure from this NW-SE orientation at the top and bottom of the Bunter shale, coinciding with zones of high vertical birefrigence. Elsewhere in the overburden the vertical birefringence is 3%. Most of the gross features of the data from the walkaway VSPs can be successfully modelled using a plane-layered model due to the structural uniformity of the survey area. In order to match the transverse component energy, it is necessary to introduce a substantial 50% vertical birefringence in the Plattendolomit layer. This result appears consistent with fracture intensities for fine-grained, low-porosity rocks with a high percentage of brittle constituents (Nelson 1985). Although there is no hard geological evidence of fracturing in this well, drilling logs revealed the intersection of permeable zones every 30 m, indicating the possibility of large productive fractures. The large recorded percentage anisotropy clearly relates to a good fracture compliance, which in turn must indicate a large open area for transmission of fluids between the fracture interfaces (Schoenberg and Sayers 1995). Unfortunately, there were no further downhole data to corroborate these findings and no available core. During drilling three particularly significant zones were intersected but the hole was eventually lost.

Summary of the benejits of this technique

The proposed technique relies upon the specific geometry of a vertical seismic profile (VSP), which benefits from a flexibility to negotiate difficult and complex faulted

zones in the North Sea. Walkaway VSPs, in particular, provide an ideal cost-effective tool for those areas where estimation of fracture details within individual fault blocks is required. This is necessary in cases where fluid flow through low-permeability rocks is dominated by the fracture processes rather than the matrix permeability. The technique relies upon the ability to acquire several walkaway lines at azimuths oblique to the maximum compressive stress or its normal, and to monitor a particularly distinctive conversion behaviour using receivers placed within the target zone. This local conversion is a useful measure of the anisotropy for the following reasons:

1 The shear-wave conversion is local, and consequently the interpretation is unaffected by the overburden anisotropy, including the near-surface and possible evaporite anisotropy.

2 The amplitude of the transverse component is a direct measure of the anisotropy in the reservoir.

3 The conversion amplitude is interpretable regardless of water-column multiples or source signature.

4 The portion of the data with the highest signal-to-noise ratio is used.

The lateral range of the technique depends upon the relative values of the V_P in the evaporites and the V_S in the dolomite. For our present work it is estimated to be a maximum of several hundred metres. The technique may also be applicable to studies of other fractured reservoirs, although it must be emphasized that the effect is specific to the evaporite / dolomite combination of seismic velocities. It is possible that other low / high contrasts generated through over-pressure, or high / low contrasts as in coals, may be responsive to this technique.

Acknowledgements

We thank Phil Wild for help with computational aspects and Neile Peake and Sue Buck of Western Atlas Wireline for discussion in early stages of the design. This work was supported by the Edinburgh Anisotropy Project (EAP) and the Natural Environment Research Council, and is published with approval from the Director of BGS, Conoco UK and its partners, and the sponsors of EAP: Amerada Hess, Amoco, BG plc, Conoco, Elf, Fina, Mobil, PGS, Phillips, Saga Petroleum, Schlumberger, Shell, Texaco, Total.

Appendix

Algebraic expression for converted shear-wave amplitude

We regard the source arrangement as a point dilatation in the water layer, with the signature of the source action being $s(t)$. A thin veneer of isotropic material is imagined to exist at the top of the target zone. An incident P-wave is first converted isotropically to an SV-wave with an amplitude $A_{P\text{-}SV}$ dependent upon the angle of incidence θ. The SV-wavefield is then incident on the anisotropic medium (Fig. 11).

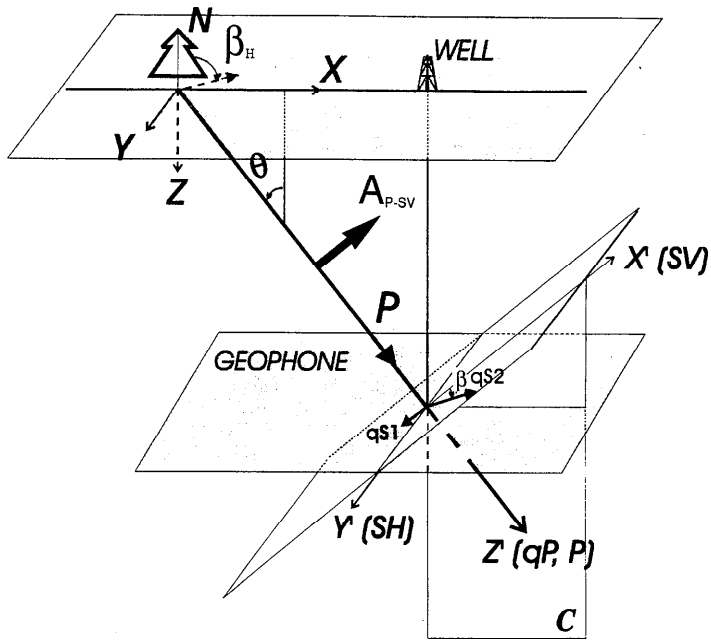

Figure 11. Geometric definitions for the parameters in (Al).

The shear-wave amplitude *u(t)* in the anisotropic medium is then found by adapting MacBeth and Li (1996), giving

$$\mathbf{u}(t) = \mathbf{R}_Y(\theta)\mathbf{R}^T_{Z'}(\beta)\Lambda_S(t)\mathbf{R}_{Z'}(\beta)\mathbf{R}^T_Y(\theta)^*\mathbf{s}_{eq}(t) \tag{A1}$$

where u(t) is measured relative to the local in-line (X) and cross-line (Y) directions, with the Z-axis pointing vertically downwards (Fig. 11). The qS2 polarization azimuth β is measured in the normal plane relative to the Y-axis, being related to the commonly measured horizontal polarization azimuth, α_H, by $\tan \alpha_H = \tan \beta \cos \theta$. $\mathbf{R}_Y(\theta)$ is a 3D rotation matrix about the fixed Y-axis, given by

$$\mathbf{R}_Y(\theta) = \begin{pmatrix} \cos\theta & 0 & -\sin\theta \\ 0 & 1 & 0 \\ \sin\theta & 0 & \cos\theta \end{pmatrix},$$

and $\mathbf{R}_{Z'}(\beta)$ is a 3D rotation matrix about the fixed Z'-axis, given by

$$\mathbf{R}_{Z'}(\beta) = \begin{pmatrix} \cos\beta & -\sin\beta & 0 \\ \sin\beta & \cos\beta & 0 \\ 0 & 0 & 1 \end{pmatrix},$$

$\Lambda_S(t)$ is a diagonal matrix containing wavelet time-shifts and amplitude factors for

propagation through the medium. The equivalent source component may be written as

$$\mathbf{s}_{\mathrm{eq}}(t) = A_{\mathrm{P-SV}}(\theta)\begin{pmatrix}\cos\theta\\0\\-\sin\theta\end{pmatrix}s(t),$$

where it is decomposed into two motions acting along the X- and Z'-axes in the dynamic plane, with no Y-component. Equation (Al) may alternatively be written as

$$\mathbf{u}(t) = A_{\mathrm{P-SV}}(\theta)\mathbf{R}_{Y}(\theta)\mathbf{R}^{T}_{Z'}(\beta)\Lambda_{\mathrm{S}}(t)\mathbf{R}_{Z'}(\beta)\begin{pmatrix}1\\0\\\mathbf{0}\end{pmatrix}. \qquad \text{(A2)}$$

References

Ahmed H. 1990. Investigation of azimuthal anisotropy from offset VSP data-a case study. *First Break 8, 449-457.*

Alford R.M. 1986. Shear data in the presence of azimuthal anisotropy: Dilley, Texas. 56th SEG meeting, Houston, Expanded Abstracts, 476-479.

Bruno M.S. and Winterstein D.F. 1994. Some influences of stratigraphy and structure on reservoir stress orientation. *Geophysics 59, 954-962.*

Fuchs K. and Schulz K. 1976. Tunneling of low-frequency waves through the subcrustal lithosphere. *Journal of Geophysics 42,* 175-190.

Guest S. and Thomson C.J. 1992. A source of significant transverse arrivals from an isotropic–anisotropic interface, e.g. the Moho. *Geophysical Journal International* 111, 309-3 18.

Horne S. and MacBeth C. 1995. Fracture characterization at the Conoco borehole test facility using shear-wave anisotropy. 65th SEG meeting, Houston, Expanded Abstracts, 426-429.

Lefeuvre F., Nicoletis L., Ansel V. and Cliet C. 1992. Detection and measurement of the shear-wave birefringence from vertical seismic data: Theory and applications. *Geophysics 57,* 1463-1481.

Lefeuvre F. and Queen J.H. 1992. Propagation matrix processing of single source 3-C VSPs. Proceedings 5IWSA, Banff. Contributions number 42.

MacBeth C. 1996. A pseudo-rotation technique for analysis of seismic anisotropy using marine VSI? 58th EAGE conference, Amsterdam, The Netherlands, Expanded Abstracts, Volume 1, co22.

MacBeth C. and Li X.-Y. 1996. Linear matrix operations for multicomponent seismic processing. *Geophysical Journal International 124,* 189-208.

MacBeth C., Wild I'., Crampin S. and Brodov L.Y. 1993. Optimal acquisition geometry determining shear-wave anisotropy. *Canadian Journal of Exploration Geophysics 29,* 132– 139.

MacBeth C., Zeng X., Li X.-Y. and Queen J. 1995. Multicomponent near-surface correction for land VSI? *Geophysical Journal International* 121, 30 l-3 15.

Mueller M. 199 1. Prediction of lateral variability in fracture intensity using multicomponent shear-wave surface seismic as a precursor to horizontal drilling in the Austin Chalk. *Geophysical Journal International* 107, 409-4 15.

Nelson R.A. 1985. *Geological Analysis of Naturally Fractured Reservoirs.* Gulf Publishing Company, London.

Schoenberg M. and Sayers C.M. 1995. Seismic anisotropy of fractured rock. *Geophysics* 60, 204-211.

Schruth P.K., Bush I. and Digranes I? 1992. Observations of shear-wave splitting from VSPs in the northern North sea. 54th EAEG meeting, Paris, France, Expanded Abstracts, PO83.

Sun Z., Brown R.J., Lawton D.C. and Wang Z. 1991. Seismic anisotropy and salt detection: A physical modelling study. 6 1 st SEG meeting, Houston, Expanded Abstracts, 7 13-7 16.

Tatham R.H. and McCormack M.D. *199* 1. *Multicomponent Seismology in Petroleum Exploration.* Society of Exploration Geophysicists.

Taylor D.B. 1987. *ANISEIS V Manual.* Applied Geophysical Software Inc.

Winterstein D.F. and Meadows M.A. 1991. Shear-wave polarizations and subsurface stress directions at Lost Hills field. *Geophysics 56,* 133 1-1348.

Zeng X. and MacBeth C. 1993. Algebraic processing techniques for estimating shear-wave splitting in near-offset VSP data: Theory. *Geophysical Prospecting* 41, 1033–1066.